Energy Conversion and Management 214 (2020) 112904

Contents lists available at ScienceDirect

Energy Conversion and Management

journal homepage: www.elsevier.com/locate/enconman

Transient search optimization for electrical parameters estimation of photovoltaic module based on datasheet values

Mohammed H. Qais[a,*], Hany M. Hasanien[b], Saad Alghuwainem[a]

[a] Electrical Engineering Department, College of Engineering, King Saud University, Riyadh 11421, Saudi Arabia
[b] Electrical Power and Machines Department, Faculty of Engineering, Ain Shams University, Cairo 11517, Egypt

ARTICLE INFO

Keywords:
Photovoltaic
Parameter estimation
Three-diode model
Transient search optimization

ABSTRACT

This paper presents a novel efficient metaheuristic algorithm called Transient Search Optimization (TSO), which is inspired by the transient process of the inductive and capacitive circuits. Also, this paper presents an objective function based on the datasheet of PV modules at standard test conditions (STC). Then, the TSO algorithm is applied to minimize the objective function to find the optimal nine parameters of the three-diode model (TDM) of the PV module. Also, the results of the proposed TSO algorithm are compared with that obtained by using other metaheuristic algorithms, where in this regard the TSO achieved the best results. The proposed technique is verified by applying it to find the optimal TDM of three commercially common PV modules with different cell types, rated power, and terminal voltage. Then, the simulated *I-V* and *P-V* characteristics of these PV modules matched with the measured data under many environmental conditions. Accordingly, the results have proved that the offered technique is useful to find the optimal TDM of all PV modules based on the dataset given by the manufacturers.

1. Introduction

The global demand for solar photovoltaic (PV) is growing due to the unsteady fossil fuel prices, political aspects, and the merits of PVs, such as size mobility, efficiency increasing, cost decreasing, and zero-emission pollutants [1]. Hence, the global installed capacity of PVs has increased, where the total power installed in 2018 is 100 [GW], as reported by the REN21 in 2019 [2]. However, there are many technical problems related to the PV panels, which are the maximum power extraction from PV panels and partial shading of PV arrays, especially for large grid-connected PV plants [3]. Therefore, an exact modeling of internal losses of the PV cells helps the researchers in simulating and overcoming these technical problems. The PV cell is a positive–negative (p-n) junction of doped semiconductor materials that converts the incident light to electrical energy. Then, the ideal electrical model of the PV cell is an electrical current source equivalent to the incident solar energy on the PV surface, which is named photo-current source. However, the exact model of the PV cell should include the internal losses of the PV cell, which are divided into electrical losses and optical losses [4]. The electrical losses can be modeled by two electrical resistances (parallel with the photo-current source and series with it). Whereas, the optical losses are the diffusion and recombination losses of the charge carriers in many regions of the PV cells, such as quasi unbiased, space charge, and deficiency regions. Hence, the optical losses can be modeled using a number of diode models (single-diode model (SDM), double-diode model (DDM), or three-diode model (TDM)). The diode model is mathematically represented by a nonlinear expression that includes an exponential function. There are two parameters for the diode model, such as the reversed-saturation current (I_o) and ideality factor (α). Therefore, the SDM model is a five-parameter model that includes photocurrent source (I_{ph}), parallel resistance (R_p), series resistance (R_s), and two parameters of a diode (I_o and α). However, the DDM is a seven-parameter model that consists of extra diode parameters more than SDM. Also, the TDM is a nine-parameter model because of the addition of the extra diode to the DDM.

In the literature review, most of the researchers focused on the SDM and DDM due to their low number of design parameters, but these models cannot be solved directly by equations analysis due to their nonlinearity. So, many papers proposed either approximated methods, iterative methods, or optimization methods to find the five parameters of SDM and seven parameters of the DDM. Moreover, some methods relied on the datasheet values at three regions, such as maximum region, short-circuit region, and open circuit region, where these data provided with the nameplate of all PV panels. Thus, these methods used approximations, such as cancelation of one resistance either series or parallel [5,6], usage of constant values for these resistances [7], usage

* Corresponding author.
E-mail addresses: mqais@ksu.edu.sa (M.H. Qais), hanyhasanien@ieee.org (H.M. Hasanien), saadalgh@ksu.edu.sa (S. Alghuwainem).

https://doi.org/10.1016/j.enconman.2020.112904
Received 27 February 2020; Received in revised form 23 April 2020; Accepted 24 April 2020
Available online 07 May 2020
0196-8904/

Nomenclature

α	Ideality factor
AM	Mass of atmosphere
E_g	Energy of band-gap (eV)
G	Solar radiation intensity (W/m^2)
I	load current of PV module (A)
I_o	Reversed saturated current (A)
I_{mpp}	Maximum power point current (A)
I_{ph}	Photocurrent (A)
$I_{s.c}$	Short-circuit current (A)
k_B	Boltzmann's parameter (1.38065e-23 J/K)
K_i , K_v	Temperature coefficients of Current and voltage (A/^{o}C, V/^{o}C)
P_{mpp}	Maximum power point power (W)
q	Charge of electrons (1.6022e-19C)
N_s	Cells No.
R_p ,R_s	parallel and series resistors (Ω)
T	PV temperature (Kelvin)
V_{mpp}	Maximum power point voltage (V)
$V_{o.c}$	Open-circuit voltage (V)
V_t	Thermal voltage (V)

Abbreviations

DDM	Double-diode model
PV	photovoltaic
SDM	Single-diode model
STC	Standard test conditions
TDM	Three-diode model
TSO	Transient search optimization

of Lambert function [8], or proposing an expression between the open-circuit voltage and ideality factor [9]. In addition, iterative methods are used to find the five-parameter model, such as Newton Raphson [10], and least mean square methods [11]. However, these methods produce approximated models with enormous errors, which are not proper for largest PV plant simulations. Therefore, most of the papers applied the optimization algorithms with the purpose of getting an accurate PV model.

The *meta*-heuristic optimization algorithms applied to estimate the electrical parameters of the nonlinear PV model. Whereas, these algorithms applied to fit the PV model with the measured data by minimizing the root of the mean-squared errors between them. So, numerous *meta*-heuristic algorithms are utilized in the estimation of SDM and DDM, such as genetic algorithm [12], harris hawk optimizer [13], adapted differential evolution algorithm [14], salp swarm optimizer [15], Jaya optimizer [16], artificial bee colony [17], whale optimization [18], firework optimizer [19], evaporating-rate-based water cycling optimizer [20], multiverse optimizer [21], cuckoo searching optimizer [22], imperialist competitive optimizer [23], and winner-leading competitive optimization [24].

Latterly, the TDM model is offered for the further precise model that can represent the internal losses of the PV module efficiently. However, the TDM is a complicated model more than the DDM and SDM, where the analytical solution is challenging. Therefore, the optimization algorithms still the only choice to attain the optimal TDM model of the PV modules. Furthermore, most of the researchers used the measured data of PV modules to find the TDM model using the root of mean-squared error concept. Hence, many *meta*-heuristic optimizers utilized in finding the nine-parameter model of PV modules, such as particle swarming optimizer [25], sunflower optimizer [26], moth-flame optimization [27,28], coyote optimizer [29], whale optimizer [30], and Harris Hawk optimization [31]. Due to the complexity of the PV model and based on the no free-lunch theory, some algorithms fail to solve the nonlinear PV model and stagnate into a local solution. So, the researchers hybridized two algorithms to achieve lower errors and better accuracy.

Merging two algorithms will create a new, stronger algorithm that has the capability of two algorithms in one algorithm called a hybridized algorithm. So, many hybridized algorithms applied to attain the SDM and DDM, such as hybridized biogeography-based optimizer with cuckoo searching optimizer [22], cuckoo optimizer with grey wolf optimization [32], simplex algorithm with flower pollination optimizer [33], Nelder-Mead with Jaya optimizer [34], artificial bee-colony with trusted-region reflected optimization [35], and whale optimizer with differential evolutionary algorithm [36]. However, the hybridization increases the computation complexity and execution time of hybrid algorithms. Furthermore, hybridization requires a higher memory capacity. Therefore, the emerging of a new *meta*-heuristic algorithm is welcomed and applied to solve engineering problems as it is expected to yield better results.

For that reason, this paper proposes a novel competent *meta*-heuristic optimizer called Transient search optimization (TSO) to find the optimal nine-parameter of the PV model. The TSO is a physics-based metaheuristic algorithm that is inspired by the transient behavior of the electrical inductive and capacitive circuits. So, the TSO is applied to minimize the proposed complex objective function based on the datasheet values. Also, the TSO is paralleled with other famous metaheuristic algorithms, such as grey wolf optimizer (GWO), whale optimization algorithm (WOA), and sunflower optimizer (SFO). Finally, The TSO and the proposed objective function are utilized for modeling three PV modules from different companies (Kyocera, Solarex, and Canadian Solar). Consequently, the I-V characteristics of the modeled PVs validated by the measured data under different temperatures and solar radiations.

The remains of the paper are organized as follows. Section 2 defines and derives the equations of the TDM model based on the datasheet values. Section 3 explains the optimization methodology, which has three subsections, where section 3.1 explains the inspiration and modeling of the TSO algorithm, section 3.2 shows the objective function, and section 3.3 shows the optimization results. Section 4 shows the simulation results compared with the measured data under different environmental conditions. Finally, section 5 gives a brief conclusion of this work.

2. Three-diode modeling of PV module

The solar radiation intensity on the surface of the PV panel is modeled in the electrical power system by a current source proportional to the radiation intensity. The losses inside the PV cell are modeled in the electrical circuit by three diodes and a resistance connected in parallel with the current source and a small resistance connected in series with them, as exhibited in Fig. 1 [25,37]. Then, the source current distributes into the three diodes, parallel resistance, and the load. Then, the load current or output current of the PV module can be expressed as in (1).

$$I = I_{ph} - I_{D1} - I_{D2} - I_{D3} - (V + IR_s)/R_p \quad (1)$$

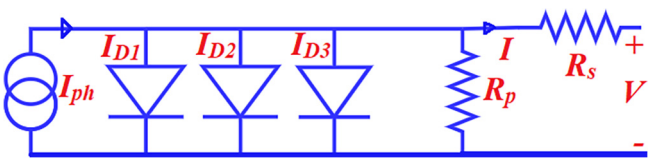

Fig. 1. TDM of PV module [25].

where the diode current is $I_D = I_0(e^{(V+IR_s)/\alpha V_t} - 1)$ and $V_t = N_s k_B T/q$.

The companies provide the data of three cases in the nameplates of the PV modules, where these cases are short-circuit point, maximum power point, and open-circuit point.

Then, many formulas can be divided from these points as follows:

Formula 1: at the short-circuit point, where $V = 0$ and $I = I_{sc}$ as follows.

$$I_{s.c} = I_{ph} - I_{D1s.c} - I_{D2s.c} - I_{D3s.c} - I_{s.c}R_s/R_p \tag{2}$$

where $I_{Ds.c} = I_0(e^{(I_{s.c}R_s)/\alpha V_t} - 1)$.

Formula 2: at the open-circuit point, where $V = V_{o.c}$ and $I = 0$ as follows.

$$0 = I_{ph} - I_{D1o.c} - I_{D2o.c} - I_{D3o.c} - V_{o.c}/R_p \tag{3}$$

where $I_{Do.c} = I_0(e^{(V_{o.c})/\alpha V_t} - 1)$.

Formula 3: at the maximum power point, where $V = V_{mpp}$ and $I = I_{mpp}$ as follows.

$$I_{mpp} = I_{ph} - I_{D1mpp} - I_{D2mpp} - I_{D3mpp} - (V_{mpp} + I_{mpp}R_s)/R_p \tag{4}$$

where $I_{Dmpp} = I_0(e^{(V_{mpp}+I_{mpp}R_s)/\alpha V_t} - 1)$.

Formula 4: the slope of power at maximum power point is zero as follows.

$$dP/dV = d(V \times I)/dV = I + VdI/dV = 0 \Rightarrow dI/dV = -I_{mpp}/V_{mpp} \tag{5}$$

Formula 5: the derivative of current can be obtained by deriving (1) as follows:

$$dI/dV = 0 - dI_{D1}/dV - dI_{D2}/dV - dI_{D3}/dV - (1 + dI/dVR_s)/R_p \tag{6}$$

Then, substitute (5) in (6) to get a new expression for the calculated (cal) maximum current point as follows.

$$I_{mpp}^{cal} = [Y_1 + Y_2 + Y_3 + (V_{mpp}/R_p)]R_p/(R_p + R_s) \tag{7}$$

where $Y = I_0\left[(V_{mpp} - I_{mpp}R_s)/\alpha V_t\right]e^{(V_{mpp}+I_{mpp}R_s)/\alpha V_t}$.

Furthermore, subtract (2) from (3) to get the calculated short-circuit current as follows.

$$I_{s.c}^{cal} = [Z_1 + Z_2 + Z_3 + (V_{o.c}/R_p)]R_p/(R_p + R_s) \tag{8}$$

where $Z = I_0\left(e^{\frac{V_{o.c}}{\alpha V_t}} - e^{\frac{I_{s.c}R_s}{\alpha V_t}}\right)$.

Then, from (7) and (8), we can formulate an expression for parallel resistance R_p as follows.

$$R_p = (V_{o.c}I_{mpp} - V_{mpp}I_{s.c})/\left[I_{s.c}(Y_1 + Y_2 + Y_3) - I_{mpp}(Z_1 + Z_2 + Z_3)\right] \tag{9}$$

where $R_p > 0$.

Then, the photocurrent can be calculated from (3) as follows.

$$I_{ph} = I_{D1o.c} + I_{D2o.c} + I_{D3o.c} + V_{o.c}/R_p \tag{10}$$

The calculated maximum power point is expressed as follows.

$$\begin{aligned} P_{mpp}^{cal} &= I_{mpp} \times V_{mpp} \\ &= V_{mpp} \times [I_{ph} - I_{D1mpp} - I_{D2mpp} - I_{D3mpp} - (V_{mpp} + I_{mpp}R_s)/R_p] \end{aligned} \tag{11}$$

Generally, all companies provide the dataset at standard test conditions (STC), where the temperature $T_{stc} = 25$ °C, the solar radiation $G_{stc} = 1$ kW/m^2, and the air mass $AM = 1.5$. Therefore, the reverse saturation current varies with the varying temperature as follows.

$$I_0 = I_0^{stc}(T/T_{stc})^3 e^{\frac{qE_g}{\alpha K_B}\left(\frac{1}{T_{stc}} - \frac{1}{T}\right)} \tag{12}$$

Also, the parallel resistance varies with the varying solar radiation as follows.

$$R_p = R_p^{stc}(G_{stc}/G) \tag{13}$$

Moreover, the photocurrent and open-circuit voltage vary with the varying temperature and solar radiation as follows.

$$I_{ph} = (I_{ph}^{stc} + K_i(T - T_{stc})) \times (G/G_{stc}) \tag{14}$$

$$V_{o.c} = V_{o.c}^{stc} + V_t \times \log\left(\frac{G}{G_{stc}}\right) + K_v \times (T - T_{stc}) \tag{15}$$

3. Optimization methodology

This section discusses the inspiration and structure of the TSO algorithm, which is applied to minimize the objective function that is proposed in this paper. Then, the optimal results and convergence curves are displayed in the last subsection.

3.1. Transient search algorithm

3.1.1. Background

The electrical circuits that are including the energy storage devices such as coils and capacitors require a period of time to reach their steady-state operation. The time period is due to the charging or discharging mechanism of the storage elements. Therefore, the circuits that contain only one storage device, as shown in Fig. 2(a), called 1st order circuit [38], where the voltage across the capacitor can be calculated as follows:

$$V_s = v_{R1} + v_1(t) = i_{c1}R_1 + v_1(t) \text{ where, } i_{c1} = C_1\frac{dv_1(t)}{dt} \tag{16}$$

$$\text{Then } \frac{d}{dt}v_1(t) + \frac{v_1(t)}{R_1C_1} = \frac{V_s}{R_1C_1} \qquad 17$$

where $v_1(t)$ is the voltage across capacitor C_1 in Fig. 2(a), R_1 is the resistance and V_s is the source voltage, then by solving the differential equation in (17), $v_1(t)$ can be expressed as follows.

$$v_1(t) = v_1(\infty) + (v_1(0) - v_1(\infty))e^{\frac{-t}{R_1C_1}} \tag{18}$$

where $v_1(0)$ is the initial capacitor voltage at time $t = 0$, and $v_1(\infty)$ is the final value of capacitor voltage.

On the other hand, the circuits that contain two storage elements, as shown in Fig. 2(b), called 2nd order circuits, where the complete response (natural response with forced response) of the voltage across the capacitor can be calculated as follows.

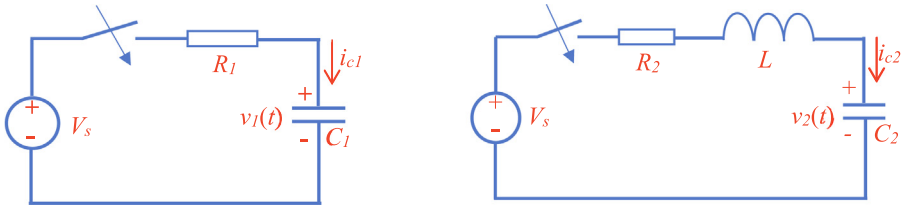

(a) (b)

Fig. 2. Electrical circuits, a) 1st order circuit, b) 2nd order circuit.

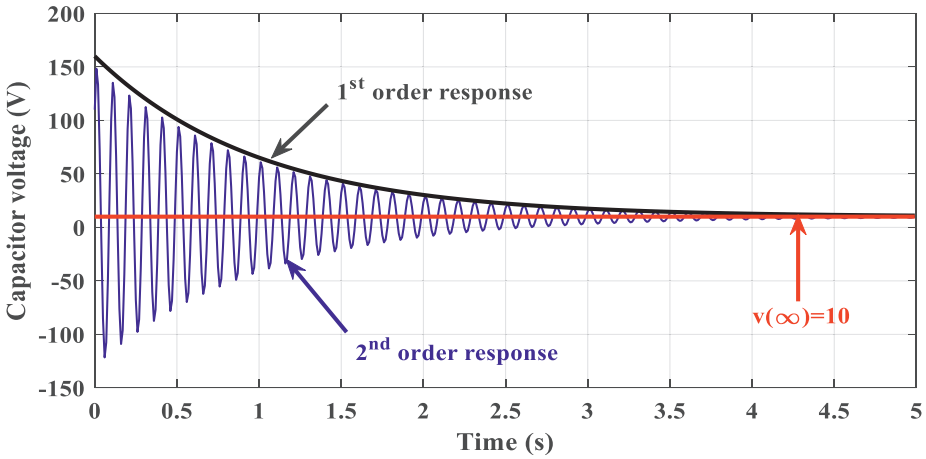

Fig. 3. Complete response of the capacitor voltage.

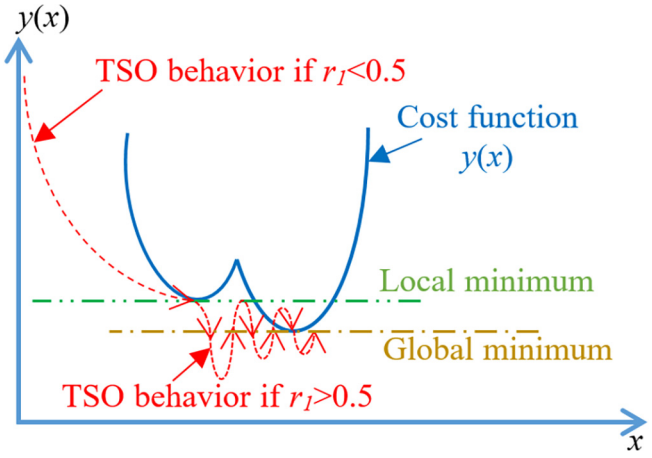

Fig. 4. TSO behavior to find the global minimum solution.

$$V_s = v_{R2} + v_L + v_2(t) = i_{c2}R_2 + L\frac{di_{c2}}{dt} + v_2(t), \text{ where } i_{c2} = C_2\frac{dv_2(t)}{dt} i_{c2} = C_2\frac{dv_2(t)}{dt} \quad (19)$$

$$\text{Then } V_s = R_2C_2\frac{d}{dt}v_2(t) + L\frac{d}{dt}\left(C_2\frac{dv_2(t)}{dt}\right) + v_2(t) \quad (20)$$

$$\text{Then } \frac{d^2}{dt^2}v_2(t) + \frac{R_2}{L}\frac{d}{dt}v_2(t) + \frac{1}{LC_2}v_2(t) = \frac{V_s}{LC_2} \quad (21)$$

where L is the inductance, and $v_2(t)$ is the voltage across the capacitor C_2. There are three solutions for the ordinary differential Eq. (21), which get underdamped, overdamped, and critical damped responses. The underdamped response solution, which is selected in this work due to the presence of oscillations, occurs when the relation in (22) is investigated. Therefore, the voltage $v_2(t)$ is expressed as in (23).

$$\left(\frac{R_2}{2L}\right)^2 < \frac{1}{LC_2} \quad (22)$$

$$v_2(t) = e^{-R_2t/2L}(B_1\cos(2\pi f_d t) + B_2\sin(2\pi f_d t)) + v_2(\infty) \quad (23)$$

where f_d is the damped frequency, B_1, and B_2 are constant coefficients.

The discharging response of the capacitor voltage for the 1st order circuit and the underdamped response of the capacitor voltage of the 2nd order circuit is displayed in Fig. 3. This figure shows that these circuits need a period of time to reach their final response, which is supposed to be 10 V. Therefore, it can be inspired by the complete response of these circuits to model a random algorithm.

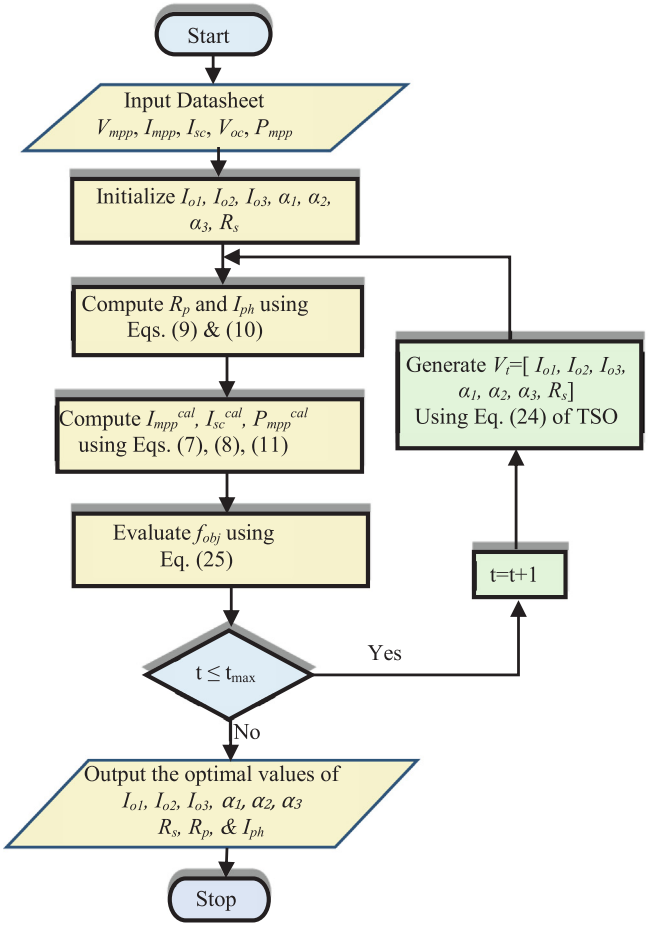

Fig. 5. The optimization Methodology Flowchart.

3.1.2. TSO modeling

The modeling of the TSO algorithm is inspired by the time response of the capacitor voltage in 1st order circuit and the underdamped response of the capacitor voltage in the 2nd order circuit. The final response of these circuits can be considered as the best solution of the TSO algorithm. The exploration behavior of the TSO algorithm is inspired by the oscillations of the underdamped response of the capacitor voltage in the 2nd order circuit. Whereas, the exploitation behavior of the TSO algorithm is inspired by the fast exponential descending of the time response of the capacitor voltage in the 1st order circuit. Then, the TSO algorithm is mathematically modeled depending on the general

Table 1
Datasheet values of PV modules under STC conditions.

Module	KC-200-GT	MSX-60	CS6K280M
Cell	Multi-crystal	Polycrystalline	Mono-crystalline
P_{mpp}	200 W	60 W	280 W
V_{mpp}	26.3 V	17.1 V	31.5 V
I_{mpp}	7.61A	3.5A	8.89A
$V_{o.c}$	32.9 V	21.1 V	38.5 V
$I_{s.c}$	8.21A	3.8A	9.43A
Cell No.	54	36	60
K_i	3.18E-03 A/°C	6.5E-02%/ °C	5.3E-02%/ °C
K_v	−1.23E-01 V/ °C	−8.0E-02 V/ °C	−3.1E-01%/ °C

Table 2
Tuning factors of algorithms.

Algorithm	Tuning factors
WOA	Constant $b = 1$ and a decreases from 2 to 0
GWO	a decreases from 2 to 0
SFO	likelihood of fertilization is 5%, $\lambda = 1$, and the number of deleted plants $m = 10\%$
TSO	$k = 0$, a decreases from 2 to 0

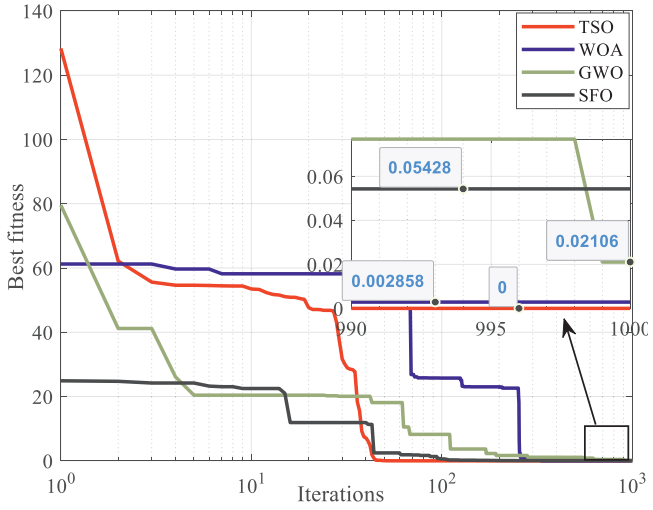

Fig. 6. Best fitness convergence with iterations for KC200GT.

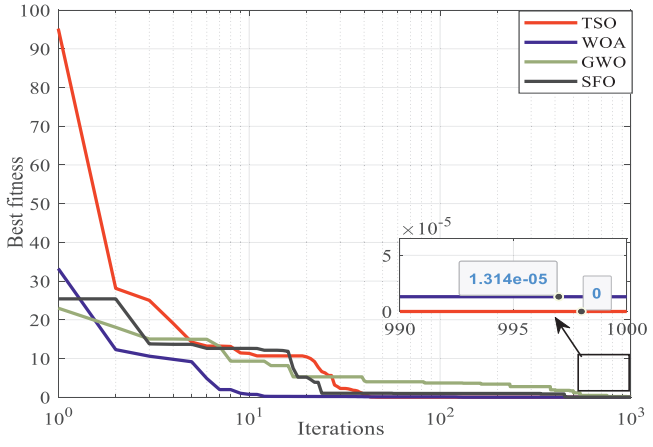

Fig. 7. Best fitness convergence with iterations for MSX-60.

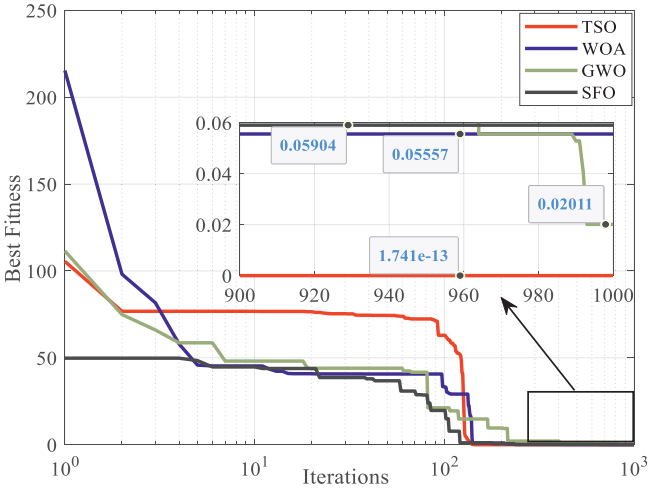

Fig. 8. Best fitness convergence with iterations for CS6K-280M.

Table 3
Optimal variables for TDM model of KC200GT.

Alg.	GWO	SFO	WOA	TSO
I_{ph} (A)	8.2209	8.21213	8.2104	8.2145
R_p (Ω)	1317.9	606.1219	947.79	466.05
R_s (Ω)	0.20322	0.23796	0.21392	0.25285
α_1	1.3141	1.2481	1.0295	1.9241
α_2	1.4503	1.991	1.00	1.5182
α_3	1.9470	1.8421	1.352	1.1905
I_{o1} (A)	6.2707e-08	4.30E-08	1.0721e-12	1.6974e-06
I_{o2} (A)	3.0069e-07	2.22E-10	1.0229e-12	8.3697e-08
I_{o3} (A)	6.7376e-07	1.35E-06	1.9751e-07	1.6316e-08
fobj	2.1062e-02	5.428e-02	2.858e-03	**0**
Time (s)	1.1749	27.15	1.2915	1.3758

Table 4
Optimal variables for TDM model of MSX-60.

Alg.	GWO	SFO	WOA	TSO
I_{ph} (A)	3.8007	3.80111	3.8012	3.8019
R_p (Ω)	434.72	578.3468	680.50	450.13
R_s (Ω)	0.27650	0.20598	0.2108	0.22724
α_1	1.9577	1.282	1.1902	1.9346
α_2	1.1324	1.8043	1.6588	1.7208
α_3	1.9674	1.4364	1.2496	1.2764
I_{o1} (A)	7.4960e-07	4.98E-08	1.6987e-12	3.3525e-07
I_{o2} (A)	6.1550e-09	7.24E-10	7.4763e-07	1.0000e-12
I_{o3} (A)	2.1717e-06	1.42E-07	3.6392e-08	6.4568e-08
fobj	4.0751e-03	1.748e-03	1.3108e-05	**0**
Time (s)	1.0360	27.25	1.3916	1.3861

Table 5
Optimal variables for TDM model of CS6K-280M.

Alg.	GWO	SFO	WOA	TSO
I_{ph} (A)	9.4392	9.440369	9.4599	9.4338
R_p (Ω)	680.38	2.16E + 04	1489.1	618.25
R_s (Ω)	0.25979	0.200	2.0128	0.2504
α_1	1.9520	2.00	1.6918	2.00
α_2	1.00	2.00	1.0064	1.0455
α_3	1.5751	1.1913	1.1890	2.00
I_{o1} (A)	8.8714e-07	1.00E-12	1.0064e-12	4.9897e-10
I_{o2} (A)	1.2987e-10	1.00E-12	1.0064e-12	3.9694e-10
I_{o3} (A)	1.4372e-09	7.46E-09	7.1114e-09	1.2678e-07
fobj	2.0107e-02	5.9040e-02	5.5567e-02	**1.7408e-13**
Time (s)	1.1171	27.18	1.3077	1.3575

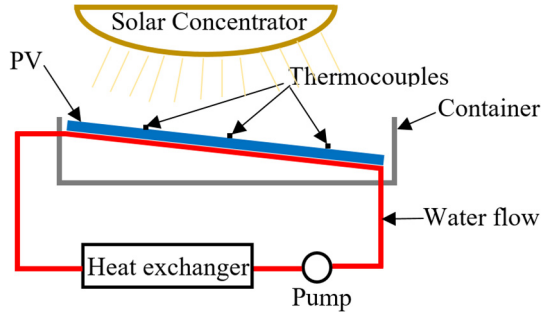

Fig. 9. Temperature and solar radiation control of the PV module.

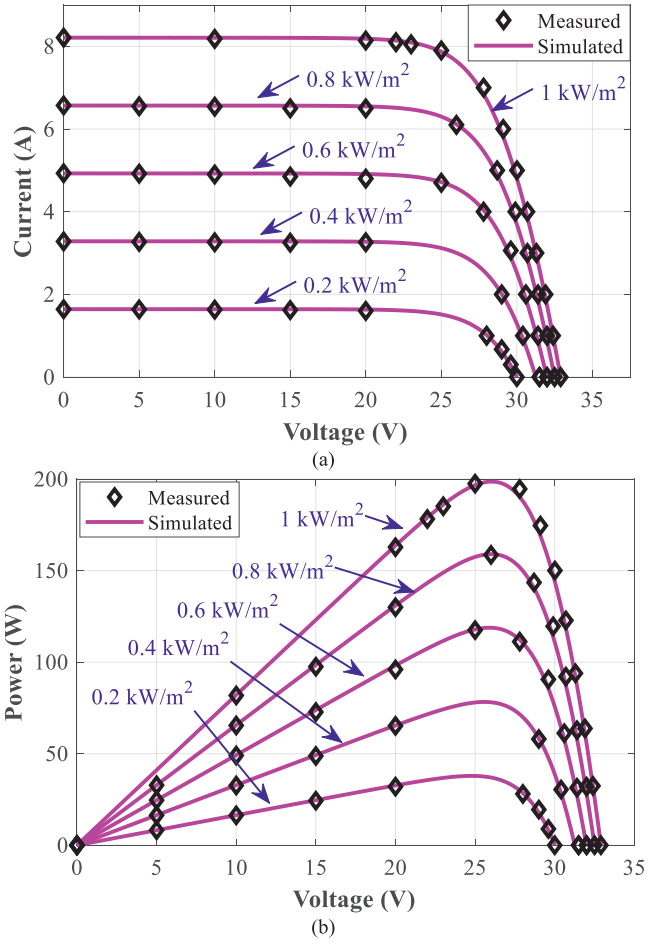

Fig. 10. KC200GT PV module characteristics a) *I-V*; b) *P-V*. at constant temperature 25 °C.

form of the Eqs. (18) and (23), where the elements (R_1, R_2, C_1, C_2, and L) are excluded to simplify the TSO algorithm. Also, the final value of capacitor voltage $v(\infty)$ is modeled as the best solution V^* and the initial value is the current iteration voltage V_t . Also, the constants B_1 and B_2 are considered as $B_1 = B_2 = |V_t\text{-}C.V_t^*|$. Therefore, the parameters of the mathematical model of the TSO algorithm are reduced as much as possible as in (24). The random number r_1 is used to balance between the exploration (searching for the optimum) and exploitation (fast convergence) of the TSO algorithm.

$$V_{t+1} = \begin{cases} V_t^* + (V_t - C.V_t^*)e^{-T} & r_1 < 0.5 \\ V_t^* + e^{-T}[\cos(2\pi T) + \sin(2\pi T)]|V_t - C.V_t^*| & r_1 \geqslant 0.5 \end{cases} \quad (24)$$

where V is the particle voltage, V^* is the final particle voltage, r_1, r_2, and r_3 are random numbers distributed uniformly between [0, 1], t is

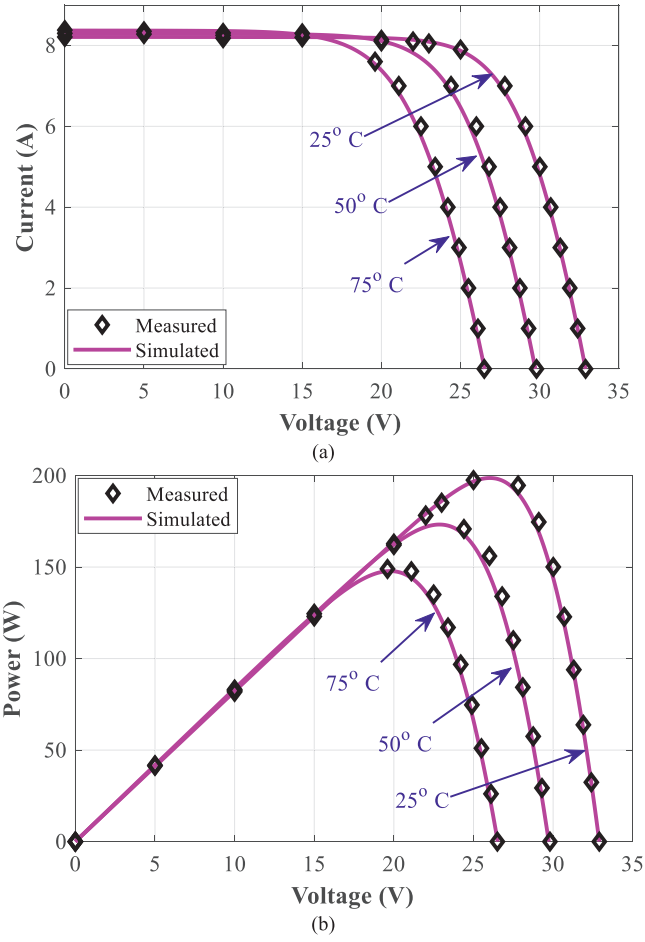

Fig. 11. KC200GT PV module characteristics a) *I-V*; b) *P-V*, at constant radiation 1 kW/m^2.

the current iteration, t_{max} is the maximum number of iterations, and k is a constant ($k = 0, 1, 2, \ldots.$), C is an element controlling the distance between the current voltage position V_t and the final voltage position V^*, which is supposed to vary between 1 and k ($C = k^*r_2^*a + 1$), a is an element proposed to control the speed convergence of the TSO algorithm, which is varying between 0 and 2 ($a = 2\text{–}2^*t/t_{max}$), and T is an element that controls the oscillation frequency of the TSO algorithm ($T = 2^*a^*r_3\text{-}a$). Fig. 4 explains how the TSO algorithm converges very fast to the location near the best solution (local minimum), then how the oscillations allow the TSO algorithm to reach the best solution (global minimum). Furthermore, the code steps of the TSO algorithm are explained in Algorithm 1.

Algorithm 1

Initialize the particle voltage between V_{min} and V_{max} as $V_0 = V_{min} + (V_{max} - V_{min})$. rand.
Evaluate the objective function of particle voltages.
Find the final voltage for the minimum objective function value.
While *($t < t_{max}$)*
Compute C_1, T, a.
  For *all particles*
    Generate the particle voltages according to Eq. (24).
  End For
Evaluate the objective function of particle voltages.
Compare the new objective function values with the stored minimum value of the objective function.
If there is a new minimum value, then update the final voltage value.
$t = t + 1$
End While
output the final particle voltage

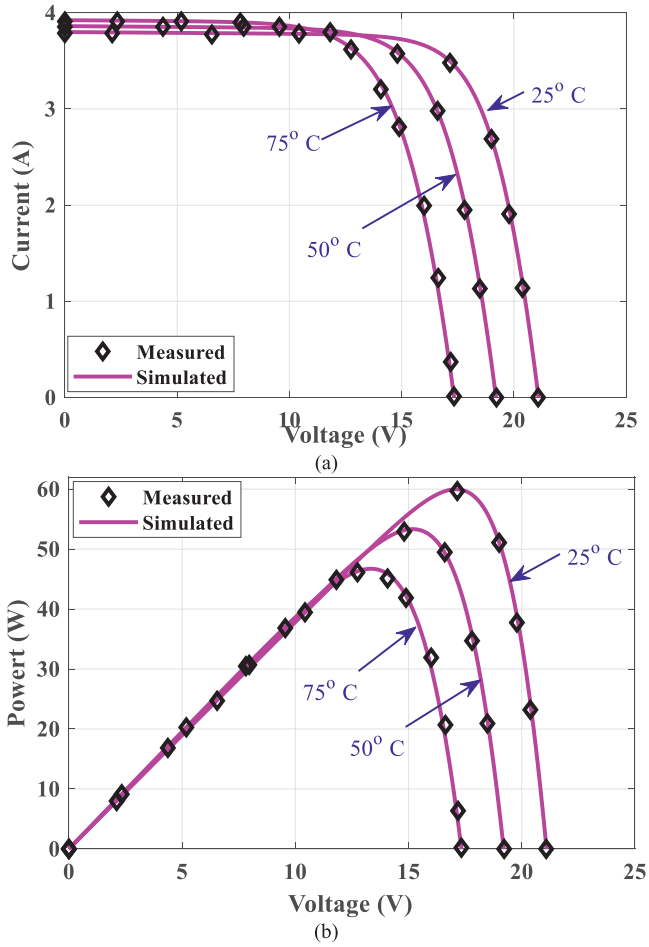

Fig. 12. MSX-60 PV module characteristics a) *I-V*; b) *P-V*, at constant radiation 1 kW/m^2.

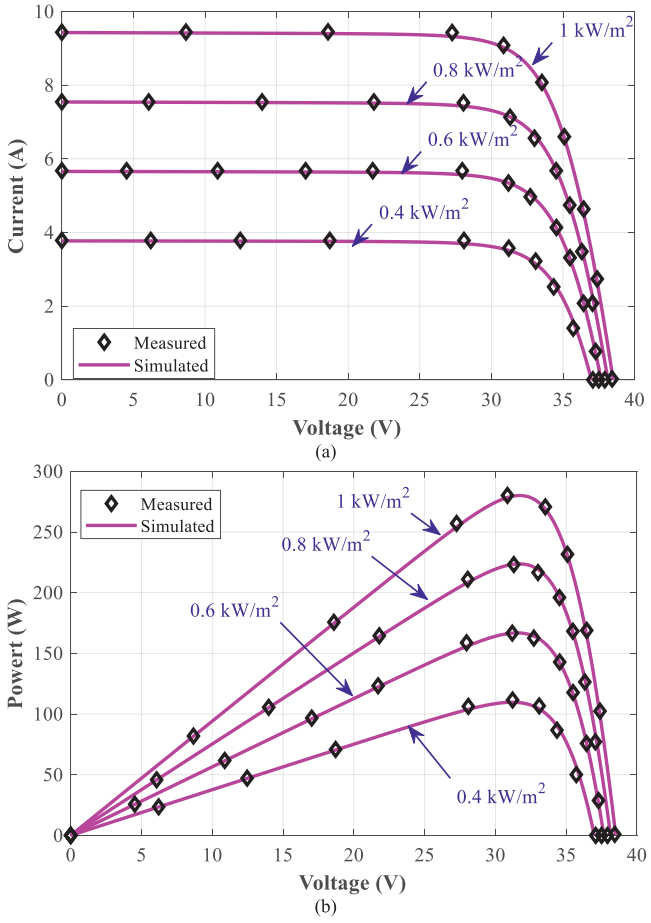

Fig. 13. CS6K-280M PV module characteristics a) *I-V*; b) *P-V*, at constant temperature 25 °C.

3.2. Objective function

The PV module established to operate at the maximum power point, then the objective function should include this point to estimate the optimal parameters of TDM. In section 2, the equations of calculating maximum current, short-circuit current, and maximum power are derived as in (7), (8), and (11), respectively. Then, the objective function is the sum of the absolute errors between the calculated values ($I_{s.c}^{cal}$, I_{mpp}^{cal}, P_{mpp}^{cal}) and the datasheet values ($I_{s.c}^{dsht}$, I_{mpp}^{dsht}, P_{mpp}^{dsht}) as in (25).

$$f_{obj}(x^T) = |I_{mpp}^{cal} - I_{mpp}^{dsht}| + |I_{s.c}^{cal} - I_{s.c}^{dsht}| + |P_{mpp}^{cal} - P_{mpp}^{dsht}| \quad (25)$$

where $x^T = [I_{o1}\ I_{o2}\ I_{o3}\ \alpha_1\ \alpha_2\ \alpha_3\ R_s\ R_p\ I_{ph}]$. the ideality factor α is between [1,2], R_s is between [0,1], the reverse saturation current I_o lies in [0, 1], R_p and I_{ph} are calculated by (9) and (10). The flowchart of optimization methodology is displayed in Fig. 5.

3.3. Optimization results

The TSO algorithm is applied to find the optimal nine-parameter of the TDM model of three commercial PV modules that have different cell types, power ratings, and voltage ratings. All companies provide the datasheet values at STC conditions in the nameplate of the PV modules. Therefore, it is preferable to find the electrical model of PVs based on datasheet values. These PV modules are produced by three famous companies, such as Kyocera (KC200GT) [39], Solarex (MSX-60) [40], and Canadian Solar (CS6K-280M) [41]. The datasheet values of these PV modules under STC conditions (G = 1 kW/m^2, T = 25 °C, and *AM* = 1.5) are displayed in Table 1.

The TSO algorithm is applied to find the optimal variables of the objective function $V^* = [I_{o1}, I_{o2}, I_{o3}, \alpha_1, \alpha_2, \alpha_3, R_s]$, that achieves zero value of the objective function. also, other *meta*-heuristic algorithms such as GWO, WOA, and SFO are applied to minimize the objective function, then the TSO compared with them. The optimization experiments performed using MATLAB 2019b [42], where 50 experiments are executed. For obtaining a fair comparison, the number of particles of all algorithms is 100 and the maximum number of iterations is t_{max} = 1000.

The tuning factors of algorithms are displayed in Table 2. The procedure of optimization is explained in the flowchart of Fig. 5. The convergence behavior of the applied algorithms toward the minimum value for KC200GT, MSX-60, and CS6K-280M are shown in Figs. 6–8, respectively. The convergence curves revealed that the TSO algorithm is competitive compared with other algorithms. The optimal variables of the objective function that are achieved by all applied algorithms for KC200GT, MSX-60, CS6K-280M are displayed in Tables 3–5, respectively. The TSO algorithm achieved the smallest value of the objective function (f_{obj}) among all applied algorithms as shown in Tables 3–5.

4. Simulation results

In this section, the optimal TDM models of the PV modules are examined under different environmental conditions, such as different ambient temperatures and different solar radiation intensities. The current–voltage (*I-V*) characteristics of the optimal TDM models are verified by using measured data of the PV modules. First of all, the experimental outdoor setup for measuring the voltages and currents of

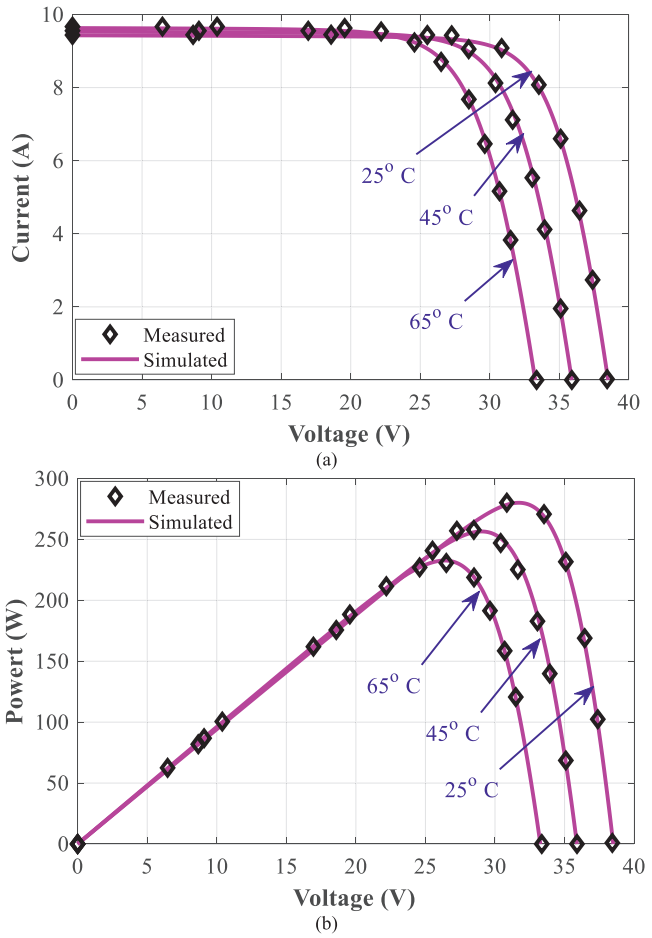

Fig. 14. CS6K-280M PV module characteristics a) *I-V*; b) *P-V*, at constant radiation 1 kW/m^2.

different PV modules (KC200GT, MSX-60, or CS6K-280M) under different environmental conditions is displayed in Fig. 9. The PV modules are placed in a container on the rooftop of the campus, where the required ambient temperature is achieved by flowing of hot or cold water in the pipes that installed behind the PV modules as illustrated in Fig. 9. The temperature of the flowing water is controlled using the coolers or heaters in the heat exchanger. The ambient temperature is measured using a high probe infrared electronic temperature gauge placed on the top of PV cell, where its accuracy is ± 1 °C and range of temperature [–32, 550 °C]. The solar radiation intensity is controlled using concentrators, which are measured using Pyranometer, where its uncertainty is ± 5% and the calibration factor of 5 W/m^2/mV. Then, the output voltage and current of PV modules measured with the digital multimeter and clamp meter. These measurements are recorded in Cairo, Egypt in June 2017.

The I-V characteristics of the PV modules simulated under different environmental conditions, then they compared with the recorded data. Firstly, the TDM model of KC200GT PV module simulated under constant temperature 25 °C and different radiation intensities (1 kW/m^2, 0.8 kW/m^2, 0.6 kW/m^2, 0.4 kW/m^2, 0.2 kW/m^2). The simulated *I-V* characteristics and *P-V* characteristics are compared with the measured data, as displayed in Fig. 10. It is noticed that the simulated results match the measured data especially the simulated maximum power matches the real maximum output power (200 [W]) at STC conditions. Furthermore, the TDM model of KC200GT simulated under different temperatures (25 °C, 50 °C, 75 °C) and constant radiation intensity 1 kW/m^2, where the simulated *I-V* characteristics and *P-V* characteristics are compared with the measured data, as displayed in Fig. 11. It can be understood from these figures that the results of the TSO-PV model are very accurate and very close to their experimental results.

Secondly, the TDM model of the MSX-60 PV module is simulated under different temperatures (25 °C, 50 °C, 75 °C) and constant radiation intensity 1 kW/m^2. The simulated *I-V* and *P-V* characteristics are plotted and compared with the measured data, as displayed in Fig. 12. It is noticed that the simulation results and measured data are highly matched and the simulated maximum power is 60 [W] at STC conditions. Thirdly, the TDM model of CS6k-280M PV module is simulated under different radiation intensities (1 kW/m^2, 0.8 kW/m^2, 0.6 kW/m^2, 0.4 kW/m^2) and constant temperature 25 °C. the simulated *I-V* and *P-V* characteristics are matched with the measured data, as displayed in Fig. 13. It is noticed that the simulation results are very close to the measured data and the simulated maximum power is 280 [W] at STC conditions. Furthermore, the TDM model of CS6K-280M is simulated under different ambient temperatures (25 °C, 45 °C, 65 °C) and constant radiation intensity 1 kW/m^2. Therefore, the *I-V* and *P-V* characteristics are matched with the measured data, as displayed in Fig. 14.

5. Conclusion

This article has proposed an accurate electrical three-diode modeling of the photovoltaic modules for electrical power system simulations. The three-diode model is a complex nonlinear model, where its electrical nine variables cannot be achieved mathematically. Therefore, the optimization algorithms are applied to solve these difficult models but some of these algorithms fail to find the global best solution due to their stagnation in the local solutions. So, this paper offered a novel optimization algorithm called Transient Search Optimization (TSO) algorithm, which is inspired by the transient performance of the electrical circuits that contain energy storage elements, such as coils and capacitors. The TSO algorithm and other algorithms, such as GWO, WOA, and SFO are applied to find the optimal variables of the proposed objective function of the TDM model for three different PV modules. The modeled PV modules (KC200GT, MSX-60, and CS6K-280M) have different cell types, power ratings, and voltage ratings. The optimization results revealed that the TSO algorithm achieved the best minimum values for the objective function among other algorithms. Also, the convergence curves show how the TSO algorithm behaves faster than other algorithms to get the best solution. Moreover, the optimal TDM models of the PV modules simulated under different environmental conditions, such as temperature and solar radiation intensity. Then, the simulated current–voltage and power-voltage characteristics of the TDM models are matched by the measured data under different conditions. In conclusion, the proposed TSO algorithm and the objective function can be exploited to find the TDM model of all commercial PV cells based on the dataset values of PVs.

CRediT authorship contribution statement

Mohammed H. Qais: Writing-original draft, Methodology, Software. **Hany M. Hasanien:** Software, Writing-review & editing. **Saad Alghuwainem:** Conceptualization, Funding acquisition, Supervision.

Declaration of Competing Interest

The authors declare that they have no known competing financial interests or personal relationships that could have appeared to influence the work reported in this paper.

Acknowledgment

The authors extend their gratitude to the Deanship of Scientific Research at King Saud University for funding this paper through research group No (RG-1440-049).

References

[1] Chen J, Yu J, Song M, Valdmanis V. Factor decomposition and prediction of solar energy consumption in the United States. J Clean Prod 2019;234:1210–20. https://doi.org/https://doi.org/10.1016/j.jclepro.2019.06.173.

[2] Renewables 2019 Global Status Report 2019:336. https://www.ren21.net/gsr-2019/ (accessed February 6, 2020).

[3] Islam Gazi, Muyeen SM, Al-Durra Ahmed, Hasanien Hany M. RTDS implementation of an improved sliding mode based inverter controller for PV system. ISA Trans. May 2016;62:50–9.

[4] Wang A, Xuan Y. A detailed study on loss processes in solar cells. Energy 2018;144:490–500. https://doi.org/10.1016/j.energy.2017.12.058.

[5] Khezzar R, Zereg M, Khezzar A. Modeling improvement of the four parameter model for photovoltaic modules. Sol Energy 2014;110:452–62. https://doi.org/10.1016/j.solener.2014.09.039.

[6] Di Piazza MC, Luna M, Petrone G, Spagnuolo G. Translation of the single-diode PV model parameters identified by using explicit formulas. IEEE J Photovoltaics 2017;7:1009–16. https://doi.org/10.1109/JPHOTOV.2017.2699321.

[7] Celik AN, Acikgoz N. Modelling and experimental verification of the operating current of mono-crystalline photovoltaic modules using four- and five-parameter models. Appl Energy 2007;84:1–15. https://doi.org/10.1016/j.apenergy.2006.04.007.

[8] Peng L, Sun Y, Meng Z. An improved model and parameters extraction for photovoltaic cells using only three state points at standard test condition. J Power Sources 2014;248:621–31. https://doi.org/10.1016/j.jpowsour.2013.07.058.

[9] Batzelis EI, Papathanassiou SA. A method for the analytical extraction of the single-diode PV model parameters. IEEE Trans Sustain Energy 2016;7:504–12. https://doi.org/10.1109/TSTE.2015.2503435.

[10] Ishaque K, Salam Z, Taheri H. Simple, fast and accurate two-diode model for photovoltaic modules. Sol Energy Mater Sol Cells 2011;95:586–94. https://doi.org/10.1016/j.solmat.2010.09.023.

[11] El Achouby H, Zaimi M, Ibral A, Assaid EM. New analytical approach for modelling effects of temperature and irradiance on physical parameters of photovoltaic solar module. Energy Convers Manag 2018;177:258–71. https://doi.org/10.1016/j.enconman.2018.09.054.

[12] Bastidas-Rodriguez JD, Petrone G, Ramos-Paja CA, Spagnuolo G. A genetic algorithm for identifying the single diode model parameters of a photovoltaic panel. Math Comput Simul 2017;131:38–54. https://doi.org/10.1016/j.matcom.2015.10.008.

[13] Chen H, Jiao S, Wang M, Heidari AA, Zhao X. Parameters identification of photovoltaic cells and modules using diversification-enriched Harris hawks optimization with chaotic drifts. J Clean Prod 2019. https://doi.org/10.1016/j.jclepro.2019.118778.

[14] Li S, Gu Q, Gong W, Ning B. An enhanced adaptive differential evolution algorithm for parameter extraction of photovoltaic models. Energy Convers Manag 2020;205:112443. https://doi.org/10.1016/j.enconman.2019.112443.

[15] Ben Messaoud R. Extraction of uncertain parameters of single and double diode model of a photovoltaic panel using salp swarm algorithm. Measurement 2019:107446. https://doi.org/10.1016/j.measurement.2019.107446.

[16] Yu K, Qu B, Yue C, Ge S, Chen X, Liang J. A performance-guided JAYA algorithm for parameters identification of photovoltaic cell and module. Appl Energy 2019;237:241–57. https://doi.org/10.1016/j.apenergy.2019.01.008.

[17] Oliva D, Cuevas E, Pajares G. Parameter identification of solar cells using artificial bee colony optimization. Energy 2014;72:93–102. https://doi.org/10.1016/j.energy.2014.05.011.

[18] Oliva D, Abd El Aziz M, Ella Hassanien A. Parameter estimation of photovoltaic cells using an improved chaotic whale optimization algorithm. Appl Energy 2017;200:141–54. https://doi.org/10.1016/j.apenergy.2017.05.029.

[19] Sudhakar Babu T, Prasanth Ram J, Sangeetha K, Laudani A, Rajasekar N. Parameter extraction of two diode solar PV model using Fireworks algorithm. Sol Energy 2016;140:265–76. https://doi.org/10.1016/j.solener.2016.10.044.

[20] Kler D, Sharma P, Banerjee A, Rana KPS, Kumar V. PV cell and module efficient parameters estimation using evaporation rate based water cycle algorithm. Swarm Evol Comput 2017;35:93–110. https://doi.org/10.1016/j.swevo.2017.02.005.

[21] Ali EE, El-Hameed MA, El-Fergany AA, El-Arini MM. Parameter extraction of photovoltaic generating units using multi-verse optimizer. Sustain Energy Technol Assessments 2016;17:68–76. https://doi.org/10.1016/j.seta.2016.08.004.

[22] Chen X, Yu K. Hybridizing cuckoo search algorithm with biogeography-based optimization for estimating photovoltaic model parameters. Sol Energy 2019;180:192–206. https://doi.org/10.1016/j.solener.2019.01.025.

[23] Fathy A, Rezk H. Parameter estimation of photovoltaic system using imperialist competitive algorithm. Renew Energy 2017;111:307–20. https://doi.org/10.1016/j.renene.2017.04.014.

[24] Xiong G, Zhang J, Shi D, Zhu L, Yuan X, Tan Z. Winner-leading competitive swarm optimizer with dynamic Gaussian mutation for parameter extraction of solar photovoltaic models. Energy Convers Manag 2020;206. https://doi.org/10.1016/j.enconman.2019.112450.

[25] Khanna V, Das BK, Bisht D, Vandana Singh PK. A three diode model for industrial solar cells and estimation of solar cell parameters using PSO algorithm. Renew Energy 2015;78:105–13. https://doi.org/10.1016/j.renene.2014.12.072.

[26] Qais MH, Hasanien HM, Alghuwainem S. Identification of electrical parameters for three-diode photovoltaic model using analytical and sunflower optimization algorithm. Appl Energy 2019;250:109–17. https://doi.org/10.1016/j.apenergy.2019.05.013.

[27] Fathy A, Elaziz MA, Sayed ET, Olabi AG, Rezk H. Optimal parameter identification of triple-junction photovoltaic panel based on enhanced moth search algorithm. Energy 2019;188:116025. https://doi.org/10.1016/j.energy.2019.116025.

[28] Allam D, Yousri DA, Eteiba MB. Parameters extraction of the three diode model for the multi-crystalline solar cell/module using Moth-Flame Optimization Algorithm. Energy Convers Manag 2016;123:535–48. https://doi.org/10.1016/j.enconman.2016.06.052.

[29] Qais MH, Hasanien HM, Alghuwainem S, Nouh AS. Coyote optimization algorithm for parameters extraction of three-diode photovoltaic models of photovoltaic modules. Energy 2019;187:116001. https://doi.org/10.1016/j.energy.2019.116001.

[30] Elazab OS, Hasanien HM, Elgendy MA, Abdeen AM. Parameters estimation of single- and multiplediode photovoltaic model using whale optimisation algorithm. IET Renew Power Gener 2018;12:1755–61. https://doi.org/10.1049/iet-rpg.2018.5317.

[31] Qais MH, Hasanien HM, Alghuwainem S. Parameters extraction of three-diode photovoltaic model using computation and Harris Hawks optimization. Energy 2020;195:117040. https://doi.org/10.1016/j.energy.2020.117040.

[32] Long W, Cai S, Jiao J, Xu M, Wu T. A new hybrid algorithm based on grey wolf optimizer and cuckoo search for parameter extraction of solar photovoltaic models. Energy Convers Manag 2020;203:112243. https://doi.org/10.1016/j.enconman.2019.112243.

[33] Xu S, Wang Y. Parameter estimation of photovoltaic modules using a hybrid flower pollination algorithm. Energy Convers Manag 2017;144:53–68. https://doi.org/10.1016/j.enconman.2017.04.042.

[34] Luo X, Cao L, Wang L, Zhao Z, Huang C. Parameter identification of the photovoltaic cell model with a hybrid Jaya-NM algorithm. Optik (Stuttg) 2018;171:200–3. https://doi.org/10.1016/j.ijleo.2018.06.047.

[35] Wu L, Chen Z, Long C, Cheng S, Lin P, Chen Y, et al. Parameter extraction of photovoltaic models from measured I-V characteristics curves using a hybrid trust-region reflective algorithm. Appl Energy 2018;232:36–53. https://doi.org/10.1016/j.apenergy.2018.09.161.

[36] Xiong G, Zhang J, Yuan X, Shi D, He Y, Yao G. Parameter extraction of solar photovoltaic models by means of a hybrid differential evolution with whale optimization algorithm. Sol Energy 2018;176:742–61. https://doi.org/10.1016/j.solener.2018.10.050.

[37] Elaab Omnia S, Hasanien Hany M, Alsaidan Ibrahim, Abdelaiz Almoataz Y, Muyeen SM. Parameter estimation of three diode photovoltaic model using grasshopper optimization algorithm. Energies January 2020;13(2):1–15. 497.

[38] Dorf RC. Introduction to Electric Circuits. 9th ed. London, UK, UK: John Wiley & Sons; 2013. https://doi.org/10.1080/03043799308928170.

[39] Kyocera. KC200GT Kyocera PV module datasheet 2018. http://www.kyocera.com.sg/products/solar/pdf/kc200gt.pdf (accessed December 1, 2018).

[40] Solarex. MSX-60 PV module Solarex datasheet 2018. http://www.solarelectricsupply.com/solar-panels/solarex/solarex-msx-60-w-junction-box (accessed December 1, 2018).

[41] CS6K-280M canadiansolar PV module datasheet n.d. https://www.canadiansolar.com/downloads/datasheets/v5.5/Canadian_Solar-Datasheets-CS6K-M-v5.52en.pdf (accessed December 1, 2018).

[42] Mathworks. Matlab2016b 2016. https://www.mathworks.com.